Simultaneous Dual-Color Amplified Spontaneous Emission and Lasing from Colloidal Quantum Well Gain Media in their Own Layered Waveguide and Cavity

*Ahmet Tarik Isik, Farzan Shabani, Furkan Isik, Satish Kumar, Savas Delikanli, and Hilmi Volkan Demir**

Micro/nanoscale semiconductor multicolor lasers offer great potential for enhanced-performance photonic circuits. Colloidal quantum wells (CQWs) are excellent candidates as active materials for these platforms owing to their superior properties including suppressed Auger recombination and large absorption cross-section. In this work, multicolor optical gain and lasing from the heterostructures of CQWs as the gain media in their own all-solution processed optical cavity are proposed and demonstrated for the first time. Here, using a simple waveguide slab consisting of the thin films of green-emitting $CdSeS/Cd_{0.1}Zn_{0.9}S$ core/hot-injection-shell grown CQWs and red-emitting CdSe/CdS@CdZnS core/crown@shell CQWs, a transparent low refractive index colloidal spacing layer of silica nanoparticles (NPs) is devised that critically suppresses otherwise detrimental nonradiative energy transfer between the green and red-emitting CQWs. This multilayer configuration is key to enabling simultaneous amplified spontaneous emission behavior in two colors with low threshold levels. This layered architecture is further adapted to a whispering-gallery-mode cavity by fabricating a microdisk pattern directly out of these CQWs-NPs-CQWs colloids. The resulting device exhibits dual-color multimode lasing both at 569 and 648 nm at the same time. This unique multicolor lasing layered architecture holds great promise for on-chip photonic applications such as dual-color biological imaging.

1. Introduction

For a few decades, intense research efforts have been conducted on semiconductor micro- and nano-lasers because of their unique advantages including their compactness, fast dynamics, and emission efficiency.[1–3] In particular, multicolor lasers have attracted great scientific interest owing to their high demand in many application fields, such as on-chip optical communication,[4] integrated photonic circuits,[5,6] biochemical sensing,[7] and biological imaging,[8] besides their high potential for realizing efficient white light generation[9] and full-color laser display.[10,11] To date, several systems of fluorescent semiconductor nanomaterials and deposition techniques have been investigated as part of the efforts to demonstrate efficient and stable multicolor lasers. Among them, group III-V quantum wells using epitaxial growth,[12] group II-VI semiconductors using chemical vapor deposition (CVD),[13] and colloidal perovskites,[14] and organic molecules[15] using spin-casting have been employed as the active media for the demonstration of multi-wavelength optical gain and lasing. To achieve the lasing at two or more different wavelengths simultaneously, different types of optical cavities such as distributed-feedback (DFB) cavity,[16] whispering-gallery-mode (WGM) cavity,[17] and nanowire[6] and nanosheet[18] self-resonant cavities have been implemented.

Solution-processable colloidal semiconductor nanocrystals offer significant potential as a gain medium for multicolor laser devices thanks to their low-cost production, easy processability, size-tunable bandgap, strong light absorption, and compatibility with several optical cavity types.[19–22] Various studies have been conducted to realize low-threshold single-color optical gain for colloidal quantum dots (QDs) and their 2D counterparts, colloidal quantum wells (CQWs).[23,24] Through the integration of these nanomaterials into different optical feedback configurations, such as Fabry–Pérot type cavity,[25] vertical cavity surface emitting laser (VCSEL),[26,27] WGM resonator,[28,29] DFB laser,[30] and single-color colloidal lasers have been demonstrated.

A. T. Isik, F. Shabani, F. Isik, S. Kumar, S. Delikanli, H. V. Demir
Department of Electrical and Electronics Engineering, Department of Physics, UNAM, National Nanotechnology Research Center and Institute of Materials Science and Nanotechnology
Bilkent University
Ankara 06800, Turkey
E-mail: volkan@bilkent.edu.tr
S. Delikanli, H. V. Demir
Luminous! Center of Excellence for Semiconductor Lighting and Displays, School of Electrical and Electronic Engineering, Division of Physics and Applied Physics, School of Physical and Mathematical Sciences, School of Materials Science and Engineering
Nanyang Technological University
Singapore 639798, Singapore

Moreover, broadband multicolor amplified spontaneous emission (ASE) and random lasing have been shown using a particular type of colloidal nanocrystals with large core and shell sizes.[31] However, these "giant" crystalline heterostructures with a high broadband spectral emission make the sensitive bandgap tuning exceedingly difficult. Also, this approach sacrifices ultra-narrowband ASE, which is one of the most attractive features of colloidal nanocrystals.

Despite all the reports on multicolor lasers, achieving multicolor optical gain and lasing using multiple bandgap tunable narrow-band materials is still challenging because of nonradiative resonance energy transfer (NRET) or, in particular, Förster resonance energy transfer (FRET).[32,33] A recent study shows that when two different colloidal nanocrystals, blue-emitting QDs and green-emitting QDs, are in the same medium, energy transfer from the blue QDs to green QDs occurs since the absorption bands of the green QDs and the emission spectrum of the blue QDs overlap.[34] This phenomenon prevents blue QDs from lasing while increasing the lasing performance of green QDs. To overcome this challenge and avoid the negative effect of FRET, a new design strategy must be developed.

Here, for the first time, we demonstrate dual-color optical gain and lasing using two active media of separate CQW thin films emitting in the green and red spectral regions. For this purpose, we proposed a structure that distances the gain media with a tunable spacing layer. In this structure, we employed green-emitting core/hot-injection-shell grown CQWs and red-emitting core/crown@shell CQWs as active materials and solution-processed SiO_2 nanoparticles (NPs) as the spacing layer. The red CQWs, SiO_2 NPs, and green CQWs were stacked by sequentially spin-casting on a fused silica substrate. Such structures with tuned thicknesses allowed us to obtain a multicolor ASE with a low threshold of ≈ 17 µJ cm^{-2}. The results confirmed the achievement of two narrowband ASE peaks in two colors, green and red. The configuration was combined with a WGM cavity to convert the ASE response into a lasing action. Our proposed multicolor microdisk cavity structure excited by femtosecond laser pulses simultaneously lases in green and red.

2. Results

To produce a dual-color lasing device, the initial step is to carefully choose two gain materials that exhibit high optical gain performance. This is essential to ensuring efficient and reliable laser operation. Additionally, the ASE thresholds of these selected gain media should be comparable to each other since the dual-color device needs to initiate lasing in both colors at approximately the same pump intensities. Here, starting with 4 monolayers (MLs) CdSe CQWs emitting at 512 nm, the emission wavelength was tuned through alloying the core and deposition of the shell. In particular, increasing the thickness of the CQWs relaxes the quantum confinement effect and results in a red shift of the original emission peak.[35] In this work, two different heterostructures were employed to ensure the highest photoluminescence quantum yield (PLQY) and chemical stability. We utilized CdSeS/Cd$_{0.1}$Zn$_{0.9}$S alloyed core/hot-injection shell and CdSe/CdS@CdZnS core/crown@shell CQWs as green and red emitters, respectively (see the Supporting Information for synthesis procedure).[36]

Both sets of CQWs have a quasi-type-II band structure, in which the electrons with a lower effective mass can leak into the shell more than holes, and also the inorganic crown and shell reduce the hole surface traps and increase the optical performance.[37] The photoluminescence (PL) and absorption spectra of the employed CQWs are presented in Figure S1 (Supporting Information). PL measurements showed that peak emission wavelengths of green and red CQWs are 575 and 642 nm, respectively. We also note that red CQWs absorb strongly in the spectral region where the green CQWs emit. This spectral overlap causes nominally strong energy transfer from green CQWs to red CQWs in close proximity and prevents us from reaching the dual-color optical gain conditions by using our in-solution CQWs in blended form.[38]

To elaborate on the optical gain behavior of our nanocrystals, we explored each CQWs by coating them on top of fused silica substrates as single thin films. For the optical gain measurements, we excited our device with a pulsed laser beam pulse width of 110 fs and 1 kHz repetition rate at the wavelength of 400 nm. During the characterization, we pumped the device by gradually increasing the excitation energy until the spectrometer was saturated. **Figure 1**b shows the intensity and FWHM of red-emitting CQWs thin film under varying pump energy. The uptrend of PL intensity starts to accelerate when the excitation energy is higher than ≈ 12 µJ cm^{-2}, which is the ASE threshold of the gain medium. After the threshold level, the full-width-at-half-maxima (FWHM) of the emission decreases from 22 to 7 nm. As seen in Figure 1a, the film exhibits red-shifted ASE spectra, with the emission peak sliding from 643 to 646 nm. This red shift experienced in the optical gain regime is a characteristic feature of quasi-type-II heterostructures.[39] Figure 1d depicts the intensity and FWHM values of the green CQWs thin film excited by a pump laser with varying energy levels. Above the ASE threshold of ≈ 9 µJ cm^{-2}, the increment of emission intensity accelerates and the FWHM reduces from 23 to 5 nm.

Avoiding energy transfer is crucial for constructing a device showing an efficient multi-color optical gain. In such a device, when the distance between two gain materials is short enough, the emergence of FRET is inevitable.[40] Therefore, separating the CQWs from each other necessitates the selection of a spacing layer with a reasonable thickness that does not allow energy transfer. One of the most critical concerns in choosing the ideal material for the spacing layer is the proportion of generated photons that couple into the active media.[41] The lower the confinement in gain media is, the higher pump energy is required to achieve optical gain. Selecting a low refractive index material for the passive spacing layer will minimize the reduction of photons coupled to active media. Hence, as the spacing layer, we decide to use SiO_2 with a refractive index of 1.48, which is smaller than the refractive index of the films of active layers. The refractive indices of the films were measured by the ellipsometry technique (Figure S2, Supporting Information). The refractive indices of the green and red thin films are found as 1.74 + i0.03 and 1.76 + i0.04 at their emission wavelength.

In our architecture, energy transfer occurs from green-emitting CQWs (donor) to red-emitting CQWs (acceptor) via FRET. Through numerical calculations, we determined the total rate of FRET for various thicknesses of the spacing layer (Figures S3 and S4, Supporting Information). As the thickness of this layer
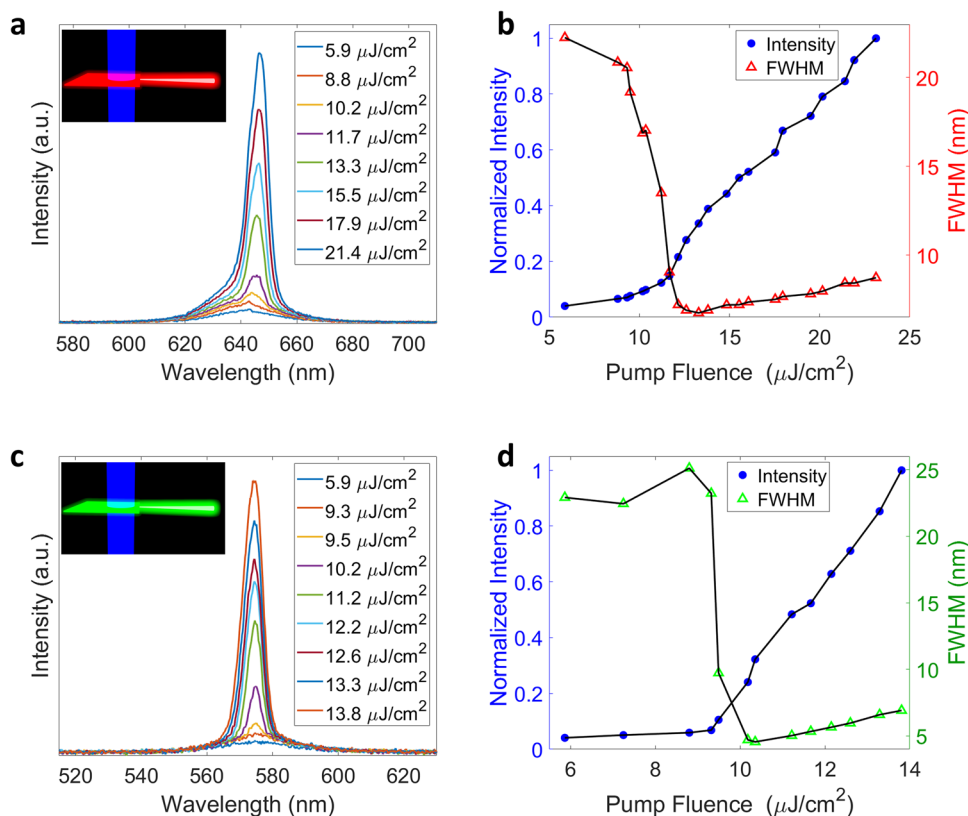
Figure 1. a) PL spectra and b) normalized peak intensities along with FWHMs of the red CQWs film under various pump intensities. ASE threshold of this film is ≈12 µJ cm⁻². c) PL spectra and d) normalized peak intensities along with FWHMs of the green CQWs film under various pump intensities. ASE threshold of this film is ≈9 µJ cm⁻². The insets display the schematics of the structures.

increased, we observed a profound decrease in the FRET rate. To achieve a FRET rate that is close to zero (practically zero), it is necessary to select a spacing layer thickness that is greater than ≈100 nm. Choosing a spacing layer thickness below ≈100 nm leads to a non-negligible amount of nonradiative energy transfer, resulting in increased optical loss and elevating the ASE and lasing threshold values.

Though it is possible to deposit SiO_2 thin film using intricate techniques such as plasma-enhanced chemical vapor deposition (PECVD), thermal evaporation, and sputtering, spin-casting solution-processable SiO_2 NPs is the most versatile method to implement a separating layer without any requirement of using high-temperature process. The solvent to disperse the SiO_2 NPs must also be carefully selected, which should be orthogonal to the solvent of the underlying film to avoid complications during the spin-casting procedure. The freedom of choice in the stabilizing ligands of the NPs allows us to use the same material in different solvent environments. We chose SiO_2 NPs dispersed in water, the orthogonal solvent for the underlying emissive layer.

Fabrication of the proposed structure started by cleaning the fused silica wafer, which is a suitable choice as the substrate since it has a low refractive index and is transparent in the visible range. Then, by employing only the spin-casting technique, we built an active-passive-active film architecture in the following order: red CQWs (50 g L⁻¹, 45 nm)/SiO_2 NPs (85 g L⁻¹, 120 nm)/green CQWs (50 g L⁻¹, 45 nm). Optical characterization of these films

was conducted following the same procedure explained above. **Figure 2**a depicts the schematic of our dual-color device under optical excitation. A detailed description of the fabrication and characterization processes can be found in Supporting Information.

The evolution of the PL spectra with pump energy is displayed in Figure 2c. In the beginning, with the low pump levels, the PL spectra present two peaks at 643 and 569 nm and relatively broadband spectra with FWHM of 26 nm for red and 30 nm for green emissions. Intensities of green and red emissions increase linearly until the excitation energy reaches a threshold, ≈16 µJ cm⁻² for the red emission and ≈17 µJ cm⁻² for the green emission (Figure 2b,d). This finding suggests, that compared to the ASE thresholds of single-layered films, the multicolor configuration shows higher threshold levels for both the red and green, individually.

For the red emission, the superiority of a single thin film over the multicolor configuration in terms of optical performance is due to the absorption and reflection that the pump laser experiences in the first and second layers (spacing layer and green CQWs) of the multilayer structure, which causes partial loss of excitation energy. However, unlike the red CQWs, the green CQWs are in the first layer of the multicolor stack, and hence pump laser interacts with it before the other layers. Therefore, green CQWs do not suffer from insufficient excitation power since they are not affected as much by the absorption and reflection of pump
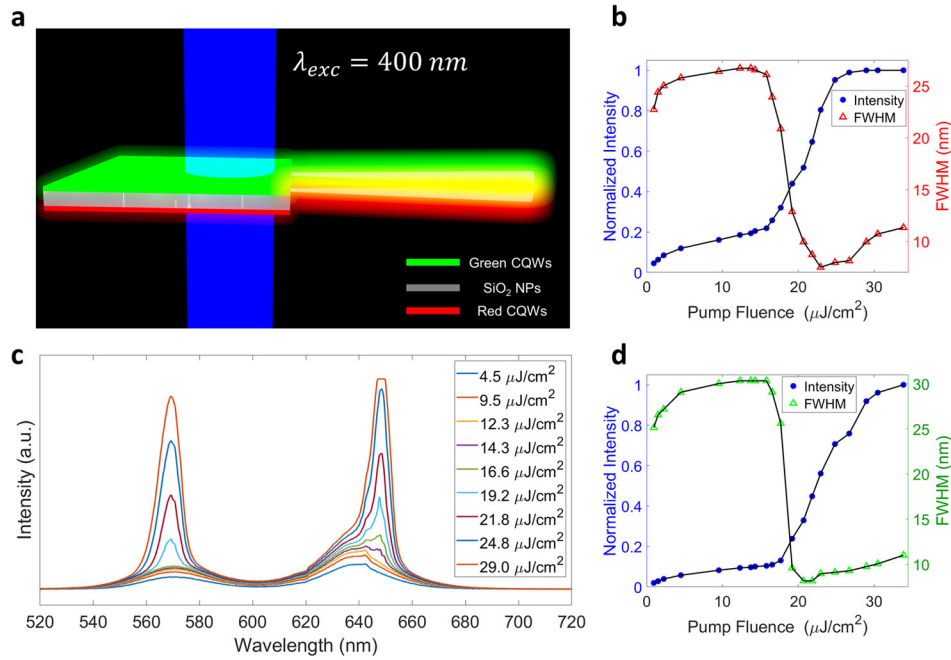
**ADVANCED
SCIENCE NEWS**

www.advancedsciencenews.com

www.lpr-journal.org

LASER
& PHOTONICS
REVIEWS

Figure 2. a) Schematic view of the multilayered film under 400 nm pump excitation showing dual-color ASE behavior. b) Normalized peak intensity and FWHM in the red spectral emission region. ASE threshold in this region is ≈16 µJ cm^{-2}. c) PL spectra of the multicolor structure under various pump intensities. d) Peak intensity and FWHM in the green spectral emission region. ASE threshold in this region is ≈17 µJ cm^{-2}.

light inside the spacing layer and red gain medium. However, in a multilayer structure, each medium introduces a certain amount of roughness due to imperfections in the coating process. The roughness accumulates with the deposition of each new layer. Since the green gain medium is the last coated layer in our multicolor configuration, it has the highest roughness. As the high optical gain requires a smooth and uniform waveguide structure, using a rough medium in ASE measurements decreases the performance.[42] This can explain the higher ASE threshold in the multicolor structure compared to the single green thin film.

In addition to the impact of roughness-induced scattering losses and decreased pump fluence, the optical performance of multilayer structures is also influenced by a reduced confinement factor as a result of incorporating another high refractive index gain medium into the structure, which decreases the overlap between each of the gain media and the associated optical modes at their respective emission wavelengths. This reduction in the confinement factor should in turn increase the ASE threshold in our multilayer structure.

Above the thresholds, we observed a slight red shift in the peak red emission wavelength from 643 to 648 nm, while the peak green emission wavelength remained the same. The amount of change is higher by 2 nm compared to the multicolor configuration. This difference is due to the size increase in the waveguide since this spectrally determines the supported mode and the modal distribution affects the peak wavelength of the ASE spectra. Besides the wavelength shift, the increase in PL intensities of green and red emissions accelerated. Also, FWHM values in two distinct spectral regions decreased drastically. PL spectra show narrowband emission ranges with FWHMs of 8 nm for both colors, indicating that the single film shows slightly narrower ASE spectra than the multicolor layer stack. This small change

can also be attributed to the evolution of modal distribution inside the waveguide. Because the multicolor structure introduces a larger waveguide size, broader ASE spectra are expected. The sharp changes in intensities and FWHMs prove that, by exciting our multicolor structure with a pump fluence level above the threshold of 17 µJ cm^{-2}, dual-wavelength ASE behavior emerges.

After showing a multicolor ASE behavior, we designed single-layer architectures by integrating our CQWs with a cavity. WGM resonator is a very suitable candidate to make the cavity out of our thin films. To have a WGM cavity, we designed a single-layered microdisk structure that includes a CQW layer. Although different types of WGM resonators, such as microspheres[11] and fiber lasers,[29] could be employed to show single-color lasing, we selected the microdisk structure due to its compatibility with our multicolor ASE configuration. The proposed microdisk laser allows for modification of the lateral axes of the ASE structure by patterning without changing the vertical axis.

We examined the lasing behavior of our CQWs by simulation, fabrication, and characterization of two different single-color microdisk structures. First, we performed a simulation utilizing finite-difference time-domain (FDTD)-based full-wave electromagnetic solutions. **Figure 3**b shows the electric-field distribution on a single-layer microdisk structure. The field is concentrated at the sides of the microdisk, thanks to the resonance presented by WGM. Based on our simulation, we fabricated and characterized two separate single-color microdisk lasers with the active media of red CQWs and green CQWs, individually. To characterize the lasing behavior of our microdisks, we excited the structures with the same laser beam used for ASE characterization. Since microdisk-type WGM resonators lase from the edges, we collected the emission from the side of the structure.
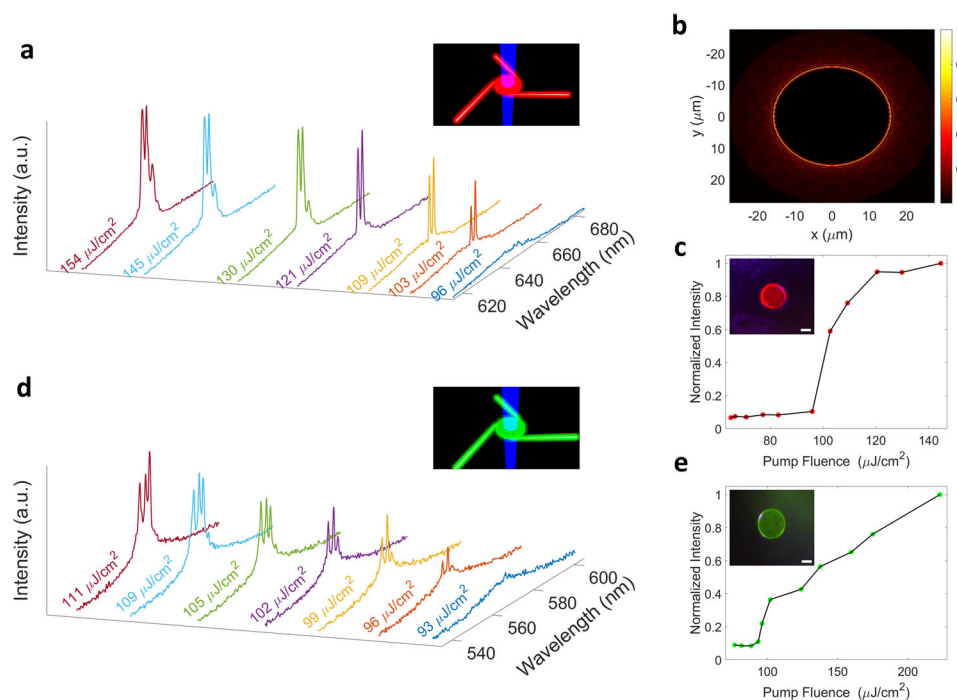
Figure 3. a) PL spectra of the single-layer red CQWs microdisk under various pump intensities. The inset displays the schematic of the structure. b) Electrical field distribution inside the microdisk obtained by 2D FDTD simulation. c) Normalized peak intensity of the red CQWs microdisk under various pump intensities. Lasing threshold of the structure is $\approx 96\ \mu\mathrm{J\ cm^{-2}}$. The inset shows the PL image of the microdisk. The scale bar is 20 μm. d) PL spectra of the single-layer green CQWs microdisk under various pump intensities. The inset displays the schematic of the structure. e) Normalized peak intensity of the green CQWs microdisk under different pump intensities. Lasing threshold of the structure is $\approx 94\ \mu\mathrm{J\ cm^{-2}}$. The inset shows the PL image of the microdisk. The scale bar is 20 μm.

Pump-dependent PL intensities of red and green lasers are presented in Figure 3c,e. The threshold level of the red laser is 96 μJ cm⁻², whereas the green laser has a threshold of 94 μJ cm⁻². We note that compared to the ASE of the red and green CQWs, with thresholds of 12 and 9 μJ cm⁻², respectively, lasing actions in microdisk structure require much higher pump energy. This rise in the threshold can be explained by the optical loss presented in the system by the WGM cavity. Although an ideal microdisk resonator does not have any cavity loss except for the outcoupling, in practice, irregularities of the optical structure introduce additional loss to the system. As can be seen in the insets of Figure 3c,e, our microdisk lasers contain imperfections around their edges. Due to the optical losses imposed by these imperfections, higher pump energy is necessary to observe lasing. Figure 3a–d shows the spectral response of PLs measured from the red and green single-color microdisk lasers.

We find the FWHMs of the structures as ≈0.9 nm for the red microdisk and ≈1.2 nm for the green microdisk. Besides, free spectral ranges (FSRs), which can be described as spacing in wavelength between two successive lasing modes, are measured to be 2.15 and 2.05 nm for the red and green lasers. As can be seen in Figure S6 (Supporting Information), we compared the measured spectral response with the results of numerical simulations and found that there was a high degree of concordance between the measured and simulated data, despite some minor discrepancies observed when comparing the two graphs, which may be attributed to variations in the sample or measurement conditions.

The achievements in showing multicolor optical gain from a well-designed multilayered structure and single-color lasing inside a WGM cavity proved that a multicolor laser can be realized via our CQWs. For this purpose, we integrated our multicolor ASE structure with a WGM cavity to concurrently observe lasing action in two separate wavelengths. To have a multicolor WGM cavity, we designed a multilayered microdisk structure that includes two active media and the spacing layer.

At the beginning of the fabrication of the multicolor laser, we coated a positive photoresist on top of a fused silica substrate and created microdisk patterns by optical lithography. Then, we subsequently filled the microdisk-shaped patterns by spin-casting the red CQWs, SiO2 NPs, and green CQWs. This multilayer architecture is the same as the multicolor ASE configuration to preserve the optical gain properties. After that, we removed the photoresist and obtained a microdisk with a diameter of 50 μm surrounded by air (see Supporting Information for details). A schematic of the microdisk laser under the optical excitation is presented in **Figure 4**a,b shows the multilayer microdisk's tilted and non-tilted scanning electron microscope (SEM) images.

The emission spectra of the multicolor microdisk WGM laser at different pump fluences are given in Figure 4c. The spectral response is the sign of a multi-mode dual-color lasing behavior since multiple lasing peaks appear in both emission regions at the pump fluences above the threshold. These lasing spectra present narrow spectral features with FWHMs of ≈2 and ≈1.5 nm for the green and red emissions, respectively. As shown in Figure 4d, the lasing threshold for both the green and red
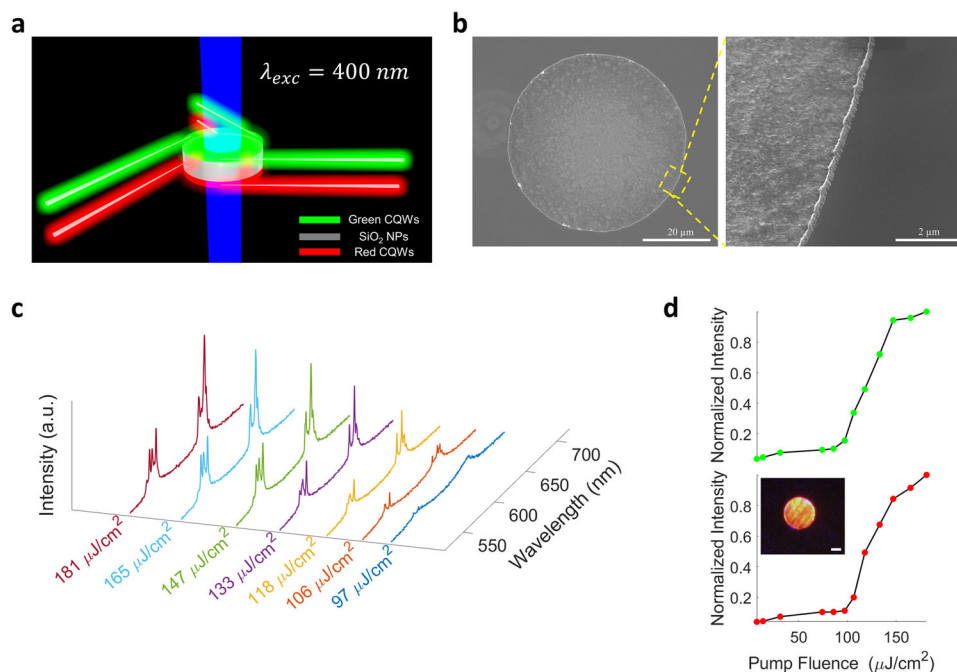
Figure 4. a) Schematic view of the multicolor microdisk architecture under 400 nm pump excitation showing dual-color lasing behavior. b) SEM images of the multilayer microdisk tilted with 0° and 52° angles. The scale bars are 20 and 2 μm, respectively. c) PL spectra of the multicolor microdisk laser under various pump intensities. d) Normalized peak intensity in green and red spectral emission regions showing that the lasing threshold is 106 μJ cm^{-2} for both colors. The inset shows the PL image of the microdisk excited by a 405 nm continuous-wave laser. The scale bar is 20 μm.

regions is observed at the pump fluence of ≈106 μJ cm^{-2} with the appearance of a narrow peak and superlinear increase of the intensity. Thus, our dual-color laser has a single threshold that is valid for both colors.

We realized that the threshold level of our multicolor laser is slightly higher than the thresholds of the single-color lasers (≈96 μJ cm^{-2}). Because each layer comes with an additional loss due to scattering and residual absorption, a multilayer structure is expected to include more losses. Indeed, a spacing layer of nanoparticles showing a vital scattering feature and the second active medium add a significant amount of optical loss to the system. This additional loss further increases the lasing threshold. Furthermore, FWHM values indicate that the multilayer architecture decreases the quality factors (Q-factors) from 722 to 433 for the red lasing and from 467 to 280 for the green lasing. Similar to the rise in the threshold level, the fall of the Q-factors is caused by the higher cavity losses of the multicolor structure. In future investigations, the quality of lasing can potentially be enhanced through a variety of approaches including utilization of an etching process leaving a smoother edge, incorporation of a flatter spacer layer between the active layers, and adaptation of other optical cavity architectures that would possibly be subject to the edge effects less and thus suffer less from the edge roughness.

3. Conclusion

In summary, we demonstrated multicolor lasing in the visible region using a novel colloidal layered architecture having all-solution-processed cavity composed of two separated CQW lay-ers for green and red emissions and a dielectric spacing layer of silica nanoparticles between these gain films, which effectively prevents degradation of the green emission by eliminating otherwise strong nonradiative energy transfer from the green to the red CQWs. We showed the achievement of multicolor ASE by exploiting these designed optical structures with a low threshold of ≈17 μJ cm^{-2}. The configuration was also integrated into a multilayered microdisk cavity acting as a WGM resonator. This architecture exhibits multi-mode lasing behavior in two colors simultaneously, with a lasing threshold of ≈106 μJ cm^{-2} in both the red and green spectral emission regions. Our findings reveal the promising potential of CQWs as the active media for multicolor optical gain applications. Moreover, relying on this low-cost and easy-fabrication method, such an all-colloidal layered laser structure is an excellent candidate for many optoelectronic applications including integrated photonic circuits and multicolor laser displays.

Supporting Information

Supporting Information is available from the Wiley Online Library or from the author.

Conflict of Interest

The authors declare no conflict of interest.

Data Availability Statement

The data that support the findings of this study are available from the corresponding author upon reasonable request.

Keywords

[1] B. R. Sutherland, E. H. Sargent, *Nat. Photon.* **2016**, *10*, 295.
[2] Y. Sun, K. Zhou, Q. Sun, J. Liu, M. Feng, Z. Li, Y. Zhou, L. Zhang, D. Li, S. Zhang, M. Ikeda, S. Liu, H. Yang, *Nat. Photon.* **2016**, *10*, 595.
[3] M. M. Adachi, F. Fan, D. P. Sellan, S. Hoogland, O. Voznyy, A. J. Houtepen, K. D. Parrish, P. Kanjanaboos, J. A. Malen, E. H. Sargent, *Nat. Commun.* **2015**, *6*, 8694.
[4] S. Han, W. Zhang, B. Qiu, H. Dong, W. Chen, M. Chu, Y. Liu, X. Yang, F. Hu, Y. S. Zhao, *Adv. Opt. Mater.* **2018**, *6*, 1
[5] M. Athanasiou, R. M. Smith, J. Pugh, Y. Gong, M. J. Cryan, T. Wang, *Sci. Rep.* **2017**, *7*, 1.
[6] C. Zhang, C. L. Zou, H. Dong, Y. Yan, J. Yao, Y. S. Zhao, *Sci. Adv.* **2017**, *3*, 1.
[7] M. Schubert, L. Woolfson, I. R. M. Barnard, A. M. Dorward, B. Casement, A. Morton, G. B. Robertson, P. L. Appleton, G. B. Miles, C. S. Tucker, S. J. Pitt, M. C. Gather, *Nat. Photonics.* **2020**, *14*, 452.
[8] T. Pan, D. Lu, H. Xin, B. Li, *Light: Sci. Appl.* **2021**, *10*, 124.
[9] A. Neumann, J. J. Wierer, W. Davis, Y. Ohno, S. R. J. Brueck, J. Y. Tsao, *Opt. Express.* **2011**, *19*, A982.
[10] J. Zhao, Y. Yan, Z. Gao, Y. Du, H. Dong, J. Yao, Y. S. Zhao, *Nat. Commun.* **2019**, *10*, 1.
[11] C. Wei, Y. Du, Y. Liu, X. Lin, C. Zhang, J. Yao, Y. S. Zhao, *J. Am. Chem. Soc.* **2019**, *141*, 5116.
[12] P. H. Dannenberg, A. C. Liapis, N. Martino, J. Kang, Y. Wu, A. Kashiparekh, S. H. Yun, *ACS Photon.* **2021**, *8*, 1301.
[13] F. Fan, S. Turkdogan, Z. Liu, D. Shelhammer, C. Z. Ning, *Nat. Nanotechnol.* **2015**, *10*, 796.
[14] M. Athanasiou, A. Manoli, P. Papagiorgis, K. Georgiou, Y. Berezovska, A. Othonos, M. I. Bodnarchuk, M. V. Kovalenko, G. Itskos, *ACS Photon.* **2022**, *9*, 2385.
[15] Y. Zhang, H. Dong, Y. Liu, C. Zhang, F. Hu, Y. S. Zhao, *Chem. Commun.* **2019**, *55*, 3445.
[16] K. Yamashita, A. Arimatsu, N. Takeuchi, M. Takayama, K. Oe, H. Yanagi, *Appl. Phys. Lett.* **2008**, *93*, 1.
[17] V. D. Ta, S. Yang, Y. Wang, Y. Gao, T. He, R. Chen, H. V. Demir, H. Sun, *Appl. Phys. Lett.* **2015**, *107*, 221103.
[18] F. Fan, Z. Liu, L. Yin, P. L. Nichols, H. Ning, S. Turkdogan, C. Z. Ning, *Semicond. Sci. Technol.* **2013**, *28*, 065005.
[19] A. L. Efros, M. Rosen, M. Kuno, M. Nirmal, D. Norris, M. Bawendi, *Phys. Rev. B Condens. Matter Mater. Phys.* **1996**, *54*, 4843.
[20] C. B. Murray, C. R. Kagan, M. G. Bawendi, *Ann. Rev. Mater. Sci.* **2000**, *30*, 545.
[21] X. Peng, L. Manna, W. Yang, J. Wickham, E. Scher, A. Kadavanich, A. P. Alivisatos, *Nature* **2000**, *404*, 59.
[22] S. Ithurria, M. D. Tessier, B. Mahler, R. P. S. M. Lobo, B. Dubertret, A. L. Efros, *Nat. Mater.* **2011**, *10*, 936.
[23] V. I. Klimov, A. A. Mikhailovsky, S. Xu, A. Malko, J. A. Hollingsworth, C. A. Leatherdale, H. J. Eisler, M. G. Bawendi, *Science* **2000**, *290*, 314.
[24] J. Lim, Y. S. Park, V. I. Klimov, *Nat. Mater.* **2018**, *17*, 42.
[25] C. Dang, J. Lee, C. Breen, J. S. Steckel, S. Coe-Sullivan, A. Nurmikko, *Nat. Nanotechnol.* **2012**, *7*, 335.
[26] S. Foroutan-Barenji, O. Erdem, S. Delikanli, H. B. Yagci, N. Gheshlaghi, Y. Altintas, H. V. Demir, *Laser Photon. Rev.* **2021**, *15*, 1.
[27] B. Guzelturk, Y. Kelestemur, M. Olutas, S. Delikanli, H. V. Demir, *ACS Nano* **2014**, *8*, 6599.
[28] W. Xie, T. Stöferle, G. Rainò, T. Aubert, S. Bisschop, Y. Zhu, R. F. Mahrt, P. Geiregat, E. Brainis, Z. Hens, D. van Thourhout, *Adv. Mater.* **2017**, *29*, 2.
[29] S. Foroutan-Barenji, F. Shabani, A. T. Isik, Z. Dikmen, H. V. Demir, *Nanoscale* **2022**, *14*, 13755.
[30] Y. Zhu, W. Xie, S. Bisschop, T. Aubert, E. Brainis, P. Geiregat, Z. Hens, D. van Thourhout, *ACS Photon.* **2017**, *4*, 2446.
[31] F. di Stasio, A. Polovitsyn, I. Angeloni, I. Moreels, R. Krahne, *ACS Photon.* **2016**, *3*, 2083.
[32] M. H. Humayun, P. L. Hernandez-Martinez, N. Gheshlaghi, O. Erdem, Y. Altintas, F. Shabani, H. V. Demir, *Small* **2021**, *17*, 2103524.
[33] N. Kholmicheva, P. Moroz, H. Eckard, G. Jensen, M. Zamkov, *ACS Energy Lett.* **2017**, *2*, 154.
[34] Y. Gao, G. Yu, Y. Wang, C. Dang, T. C. Sum, H. Sun, H. V. Demir, *J. Phys. Chem. Lett.* **2016**, *7*, 2772.
[35] M. Nasilowski, B. Mahler, E. Lhuillier, S. Ithurria, B. Dubertret, *Chem. Rev.* **2016**, *116*, 10934.
[36] Y. Altintas, K. Gungor, Y. Gao, M. Sak, U. Quliyeva, G. Bappi, E. Mutlugun, E. H. Sargent, H. V. Demir, *ACS Nano* **2019**, *13*, 10662.
[37] F. Shabani, H. Dehghanpour Baruj, I. Yurdakul, S. Delikanli, N. Gheshlaghi, F. Isik, B. Liu, Y. Altintas, B. Canımkurbey, H. V. Demir, *Small* **2022**, *18*, 2106115.
[38] L. Cerdán, E. Enciso, V. Martín, J. Bañuelos, I. López-Arbeloa, A. Costela, I. García-Moreno, *Nat. Photon.* **2012**, *6*, 621.
[39] Y. Gao, M. Li, S. Delikanli, H. Zheng, B. Liu, C. Dang, T. C. Sum, H. V. Demir, *Nanoscale* **2018**, *10*, 9466.
[40] B. Guzelturk, H. V. Demir, *Adv. Funct. Mater.* **2016**, *26*, 8158.
[41] O. Erdem, S. Foroutan, N. Gheshlaghi, B. Guzelturk, Y. Altintas, H. V. Demir, *Nano Lett.* **2020**, *20*, 6459.
[42] B. Guzelturk, Y. Kelestemur, M. Olutas, Q. Li, T. Lian, H. V. Demir, *J. Phys. Chem. Lett.* **2017**, *8*, 5317.